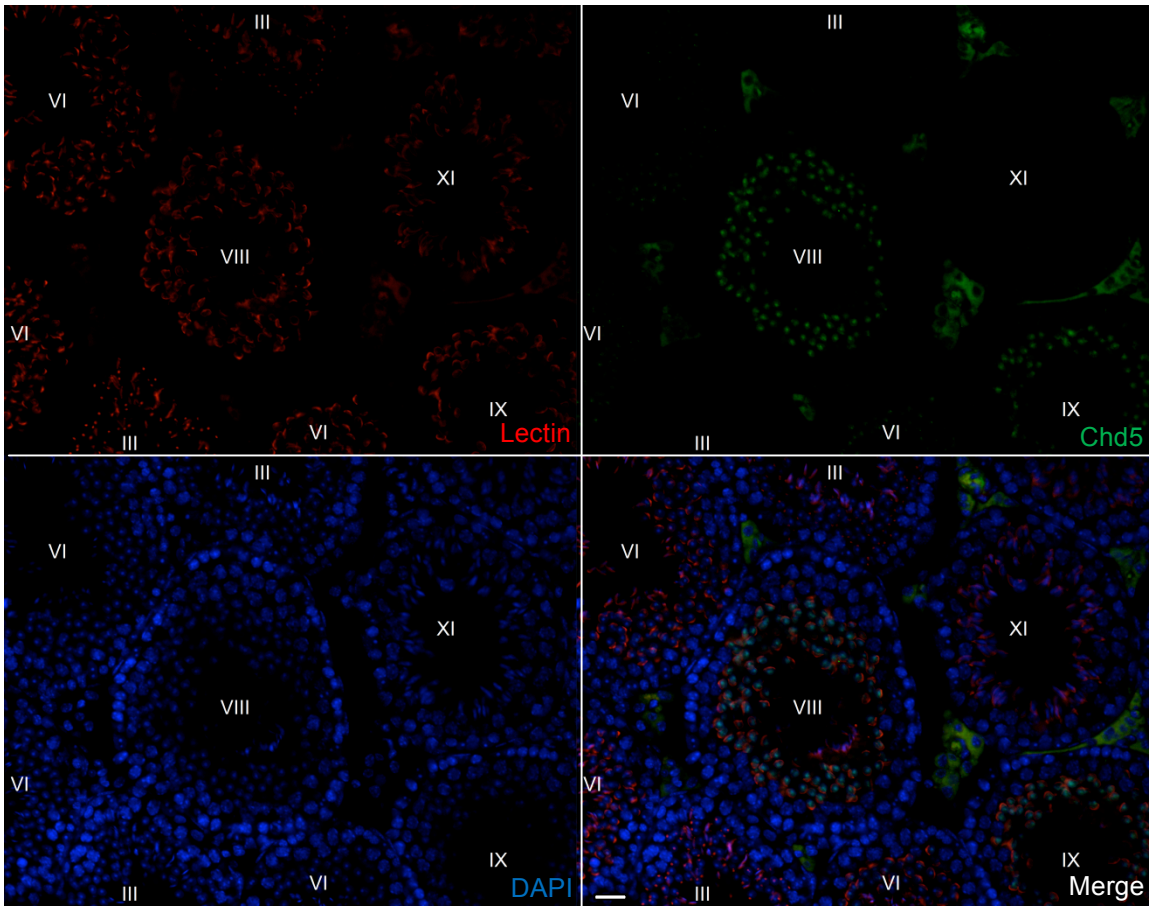

Supplementary Figure 1. Chd5 is specifically expressed in round and early elongating spermatids

Immunofluorescence of wild type mouse testes. Red, Lectin (visualizing acrosomes for staging seminiferous tubules); Green, Chd5; Blue, DAPI; Roman numerals, stage designation of the seminiferous tubules. Chd5 is specifically detected in mid-to-late round spermatids and early elongating spermatids, with peak expression in round spermatids of stage VIII tubules. Scale bar, 20 μm.

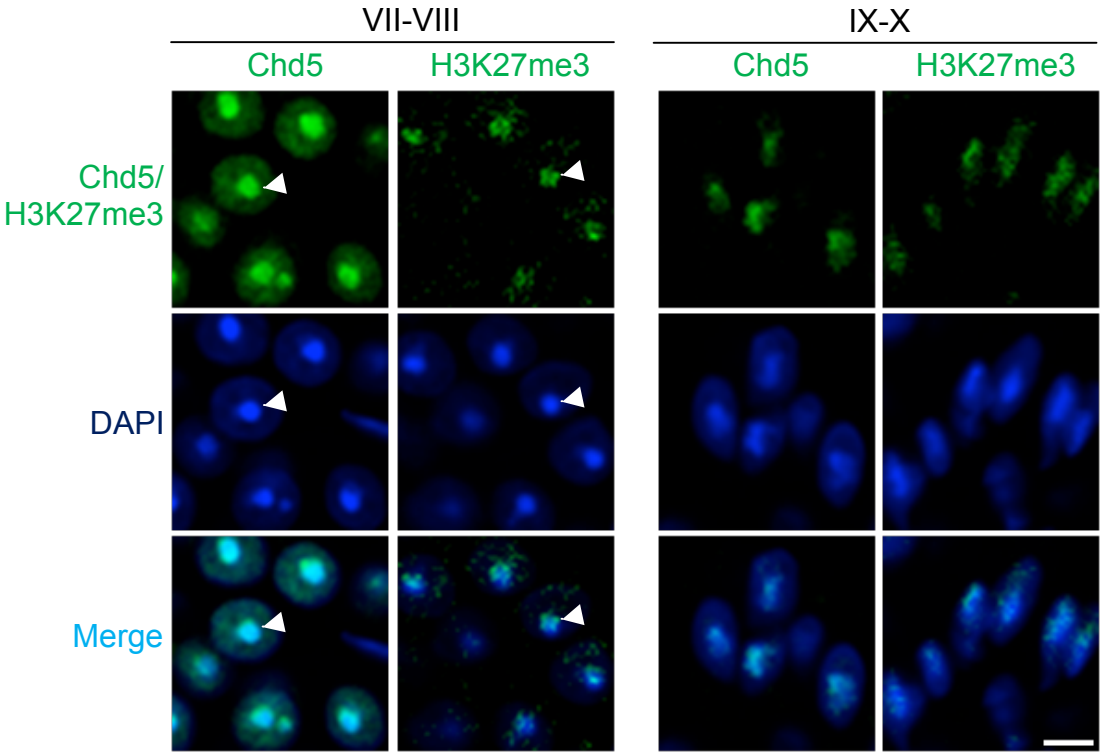

Supplementary Figure 2. Chd5 is expressed in a similar pattern as H3K27me3 in round and elongating spermatids
Immunofluorescence of wild type testes indicates that Chd5 and H3K27me3 are enriched in the heterochromatic chromocenter of round spermatids and DAPI-intense heterochromatic region of early elongating spermatids. Roman numerals indicate spermatogenic stages. Arrow heads mark chromocenter. Scale bar, 5 µm.

a

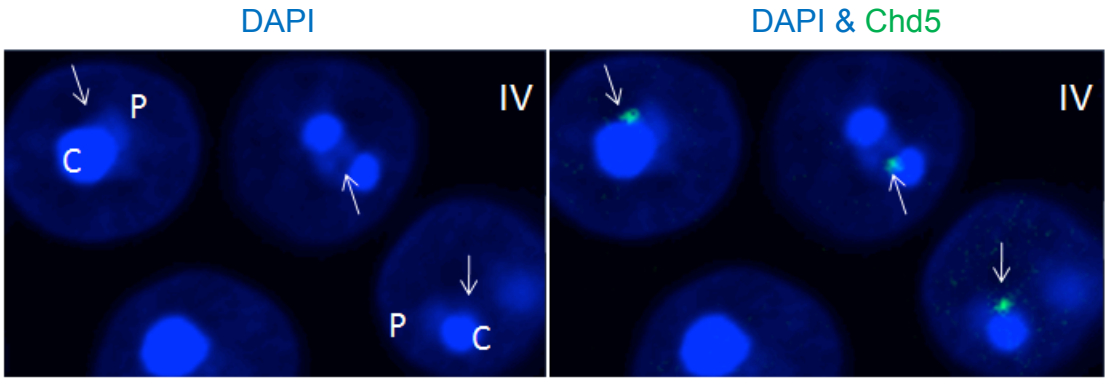

b

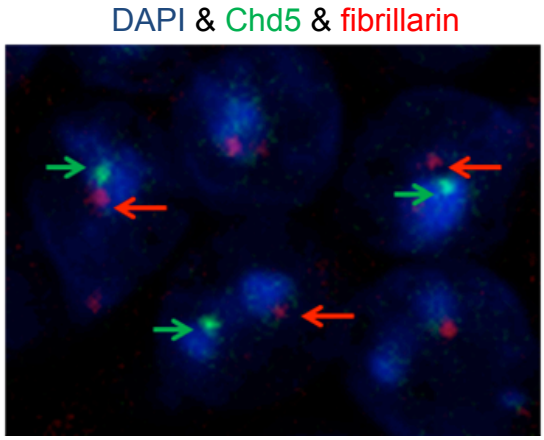

Supplementary Figure 3. Chd5 is expressed in a focal spot near the nucleolus
(**a**) Immunostaining of wild type testes revealed that an intense Chd5 spot is located at the junction of the chromocenter and the post-meiotic sex chromosome, both of which are DAPI-intense sub-nuclear regions. Blue, DAPI; Green, Chd5; C, chromocenter; P, post-meiotic sex chromosome (PMSC)[1]; IV, spermatogenic stage IV. (**b**) Co-immunostaining for Chd5 and the nucleolar marker fibrillarin indicates that Chd5-intense foci are near nucleoli in some spermatids. Blue, DAPI; Green, Chd5; Red, fibrillarin. Arrows depict spots of intense Chd5 (green) or fibrillarin (red) expression.

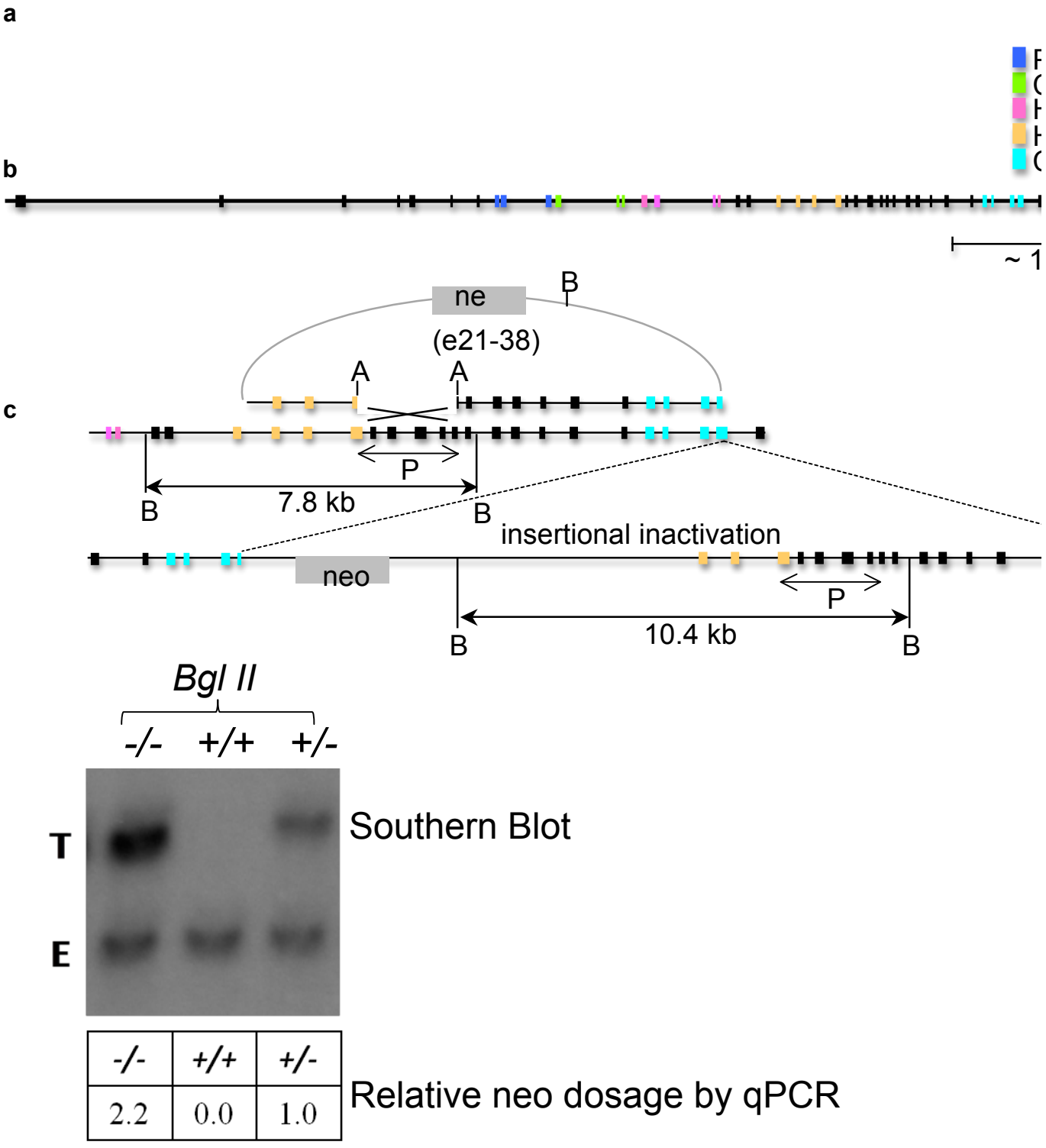

Supplementary Figure 4. Generation of *Chd5*^{Aam1} mice through gene targeting
(**a**) Genomic structure of the mouse *Chd5* gene. Exons encoding predicted functional domains are marked by colors. (**b**) Diagram of the insertion targeting vector, and the

wild-type and targeted *Chd5*^{Aam1} alleles. A, *Afl* II; B, *Bgl* II; P, location of the 2.6 kb probe for Southern blot; neo, neomycin cassette. (**c**) Top panel, Southern blot analysis of *Bgl* II digested DNA from *Chd5*$^{Aam1+/+}$ *(+/+)*, *Chd5*$^{Aam1+/-}$*(+/-)* and *Chd5*$^{Aam1-/-}$*(-/-)* mice. T, targeted band (10.4 kb); E, endogenous band (7.8 kb). The *Chd5*$^{Aam1-/-}$ lane has a more intense targeted band relative to the *Chd5*$^{Aam1+/-}$ lane, as *Chd5*$^{Aam1-/-}$ cells have two copies of the targeted 10.4 kb band while *Chd5*$^{Aam1+/-}$ cells have only one copy. The endogenous band serves as a loading control. Bottom panel, quantification of dosage of the neomycin cassette by qPCR is used for genotyping.

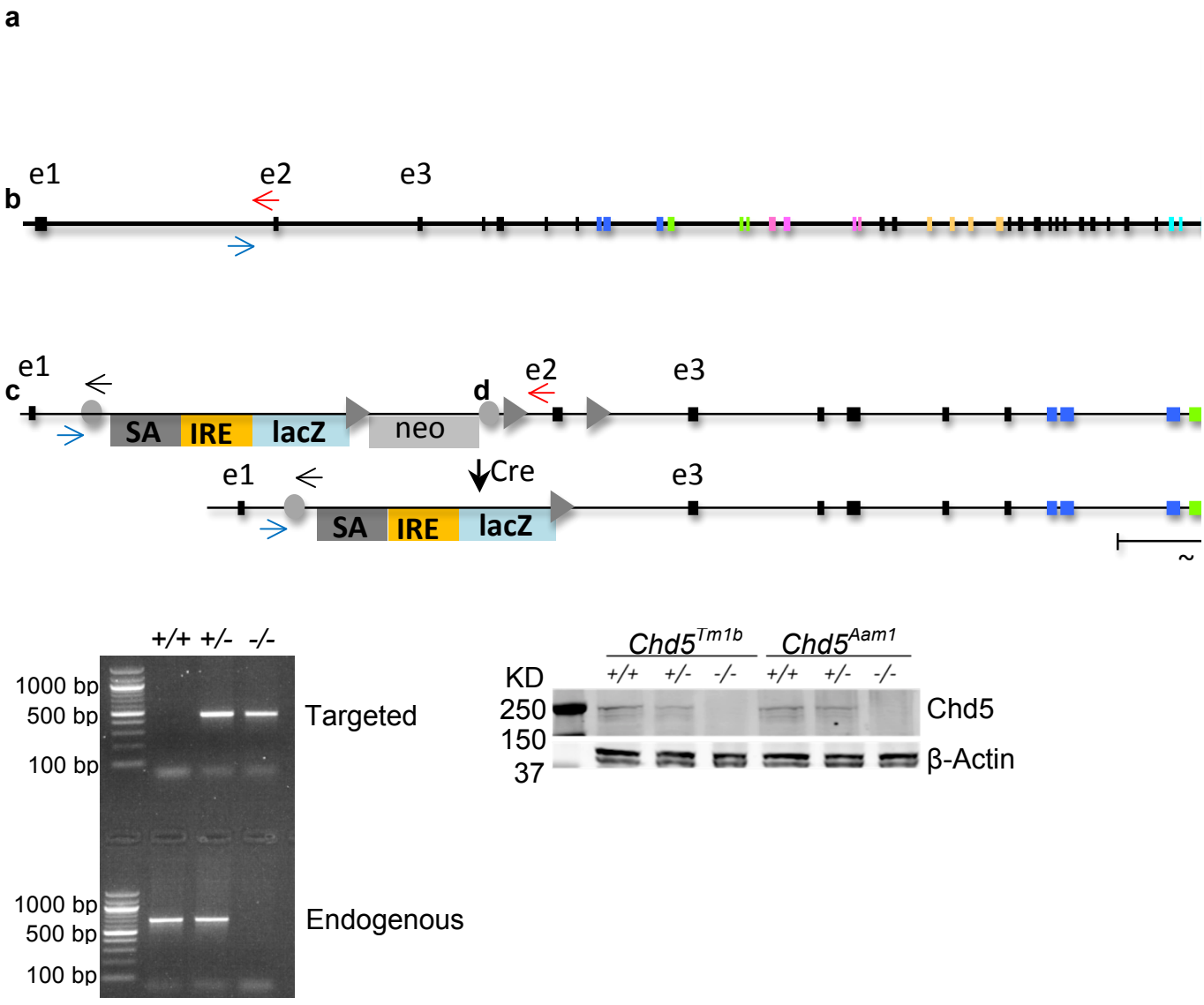

Supplementary Figure 5. Generation of *Chd5*^{Tm1b} mice through gene targeting
(**a**) Genomic structure of the mouse *Chd5* gene. Exons encoding predicted functional domains are marked by colors. Blue and red arrows indicate the PCR genotyping primers used to detect the 674 bp endogenous band specific for wild type *Chd5* allele. (**b**) Diagram of targeted *Chd5* alleles prior to (*Chd5*^{Tm1a}) and following (*Chd5*^{Tm1b}) Cre-mediated excision. Excision of exon 2 leads to a frame shift. Gray circle, *Frt* site; gray triangle, *LoxP* site; SA, splicing acceptor site; IRES, Internal ribosome entry site; lacZ, β-galactosidase; Neo, neomycin cassette. Blue and black arrows indicate the PCR genotyping primers used to detect a 456 bp band specific for the *Chd5*^{Tm1b} allele. (**c**) PCR genotyping of *Chd5*$^{Tm1b+/+}$, *Chd5*$^{Tm1b+/-}$ and *Chd5*$^{Tm1b-/-}$ mice using the primers indicated in **a, b.** Blue forward primer, Tm1b-F; black reverse primer, Tm1b-R; red reverse primer, Tm1b-WT-R. +/+, *Chd5*$^{Tm1b+/+}$; +/-, *Chd5*$^{Tm1b+/-}$; -/-, *Chd5*$^{Tm1b-/-}$. (**d**) Absence of Chd5 protein in *Chd5*$^{Tm1b-/-}$ testes. Western blot for Chd5 on total testis lysates from *Chd5*$^{Tm1b-/-}$ and *Chd5*$^{Aam1-/-}$ mice indicate that Chd5 protein is not detected in either *Chd5* null model, whereas it is detected in wild type as well as in *Chd5*$^{Tm1b+/-}$ and *Chd5*$^{Aam1+/-}$ testes. β-Actin serves as a loading control.

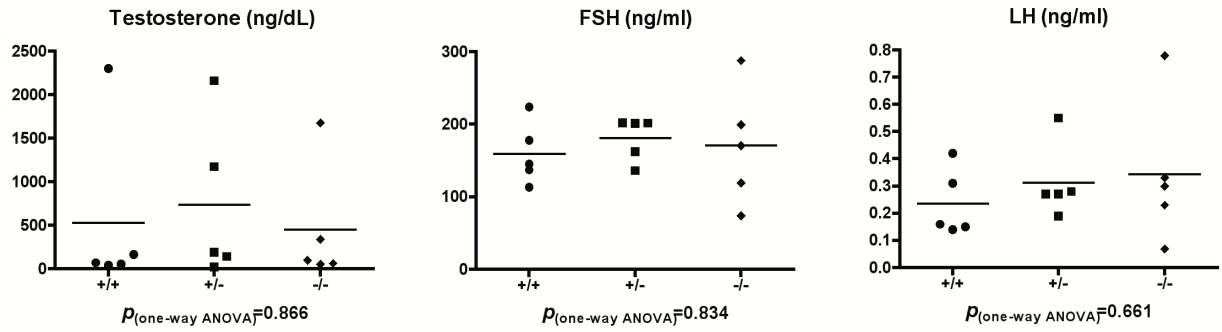

Supplementary Figure 6. No significant change in serum sex hormone levels are detected in *Chd5*$^{Aam1-/-}$ male mice
Sera were prepared from cohorts of male mice with the indicated genotypes, and levels of follicle-stimulating hormone (FSH), leutinizing hormone (LH) and testosterone examined by the Ligand Core Laboratory at University of Virginia. Each symbol represents an individual male mouse, and the horizontal bar denotes the mean of the group. Data were analyzed by one-way ANOVA. No statistically significant difference was observed among the three genotypes. +/+, *Chd5*$^{Aam1+/+}$; +/-, *Chd5*$^{Aam1+/-}$; -/-, *Chd5*$^{Aam1-/-}$.

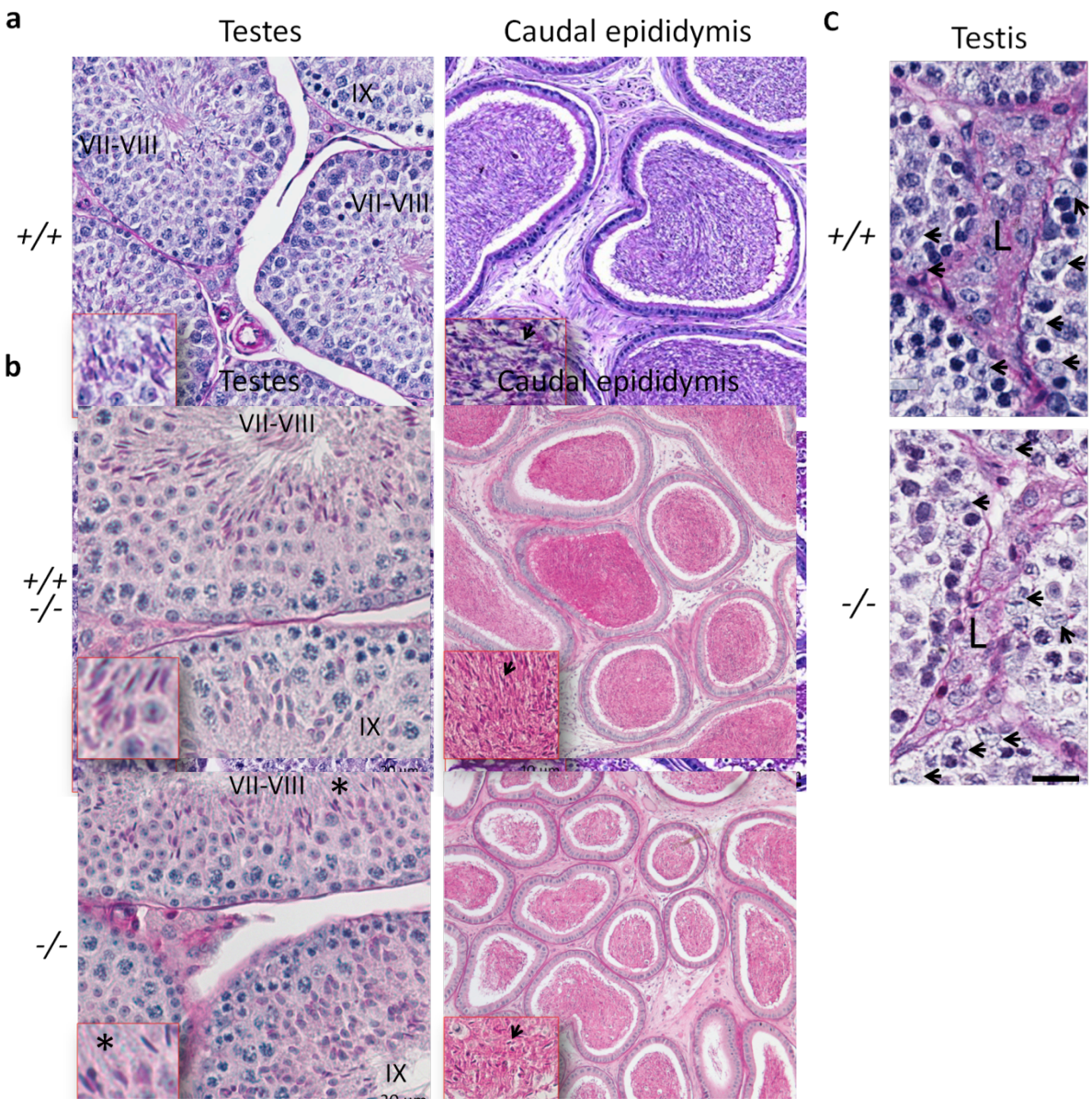
a
Testes
Caudal epididymis
c
Testis
+/+
b
IX
VII-VIII
VII-VIII
Testes
Caudal epididymis
+/+
-/-
VII-VIII
IX
VII-VIII
*
-/-
*
IX
+/+
L
-/-
L

Supplementary Figure 7. Histological analyses show variable degrees of spermatogenic defects in *Chd5*$^{Aam1-/-}$ mice

(**a**) PAS stained testes and caudal epididymis of *Chd5*$^{Aam1+/+}$ *(+/+)* and *Chd5*$^{Aam1-/-}$ *(-/-)* mice. Roman numerals indicate the stages of the seminiferous tubules. The inserts are magnified views of representative areas. * indicates that fewer spermatids are present in *Chd5*$^{Aam1-/-}$ tubules relative to *Chd5*$^{Aam1+/+}$ tubules of the same stages. Arrows depict sperm within the caudal epididymis. Note that sperm are not present in *Chd5*$^{Aam1-/-}$ caudal epididymis. (**b**) Similar but less severe histopathology in a different *Chd5*$^{Aam1-/-}$ mouse. Sperm are present in the *Chd5*$^{Aam1-/-}$ caudal epididymis, but there are fewer sperm compared to the wild type control. (**c**) No significant difference is seen in Sertoli cells (arrows) or Leydig cells (L-marked regions) between *Chd5*$^{Aam1+/+}$ and *Chd5*$^{Aam1-/-}$ testis.

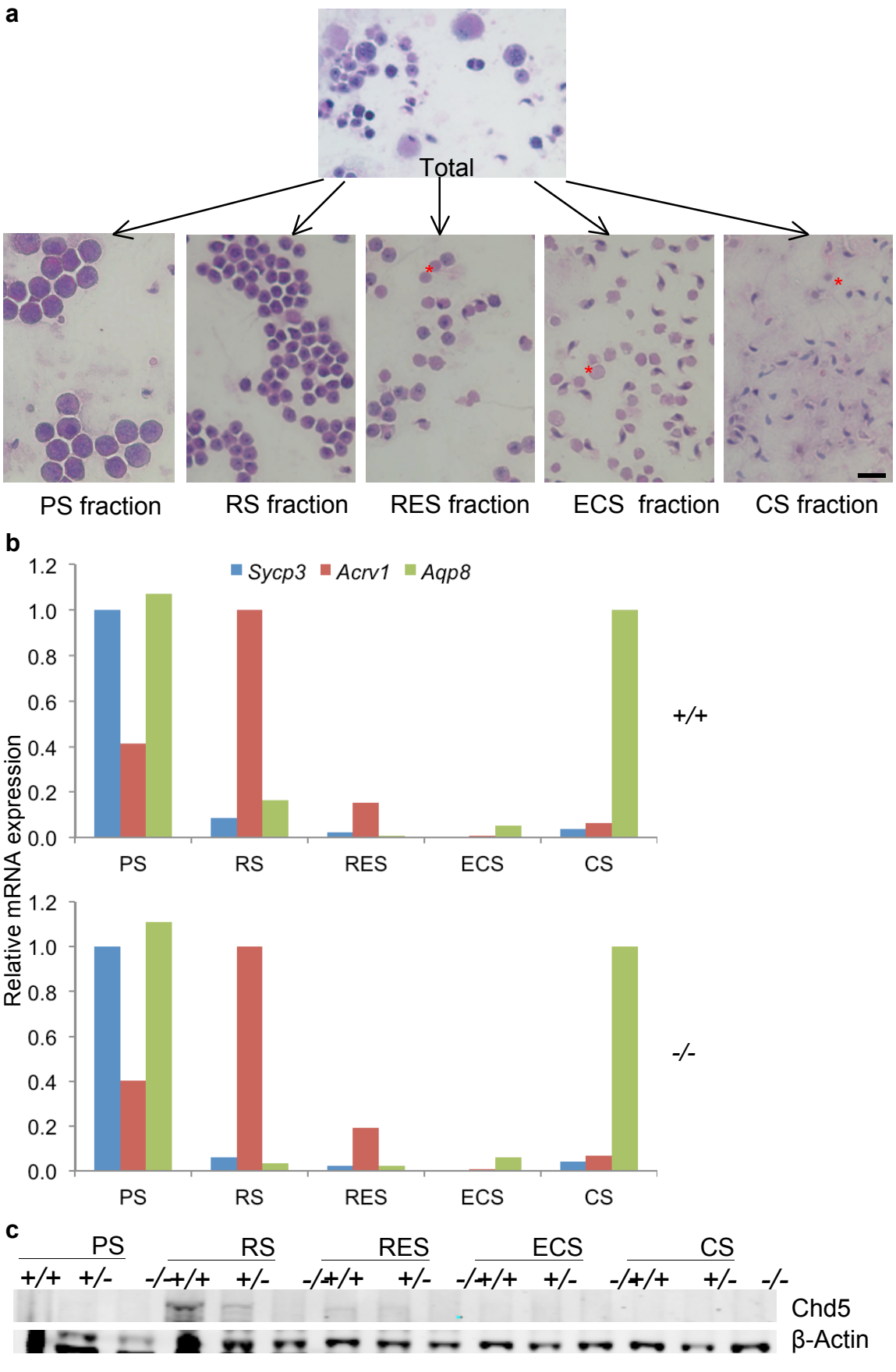
a
Total
PS fraction
RS fraction
RES fraction
ECS fraction
CS fraction
b
Sycp3
Acrv1
Aqp8
Relative mRNA expression
1.2
1.0
0.8
0.6
0.4
0.2
0.0
PS
RS
RES
ECS
CS
+/+
-/-
c
PS
RS
RES
ECS
CS
+/+ +/- -/- +/+ +/- -/- +/+ +/- -/- +/+ +/- -/- +/+ +/- -/-
Chd5
β-Actin

Supplementary Figure 8. High-purity fractions of testicular cells at different stages obtained through centrifugal elutriation

(**a**) Periodic acid–Schiff (PAS) staining of elutriation-purified testicular cell fractions. PS, pachytene spermatocytes; RS, round spermatids; RES, round and early elongating spermatids; ECS, elongating and condensing spermatids; CS, condensed spermatids. * indicates residual body. Scale bar, 10 μm. Smears were prepared from each fraction, stained with PAS and assessed for purity by counting at least 200 cells. The purities of PS, RS, ECS and CS fractions were 73%, 91%, 91% and 90% respectively. Note that the pink round bodies (as indicated by *) in RES, ECS and CS fractions are not cells, but are residual bodies of cytoplasm shed from nuclei of elongating and condensing spermatids. (**b**) Quantitative RT-PCR (qRT-PCR) analyses for stage-specific markers confirms the purity of elutriated testicular cell fractions from $Chd5^{Aam1+/-}$ (+/+) and $Chd5^{Aam1-/-}$ (-/-) testes. The expression of the marker for a specific stage, e.g. *Acrv1* expression in RS population, was defined as 1, and was used to normalize expression to other stage-specific markers. The relatively low expression of markers for other stages indicates a lack of contamination of cells from the other spermatogenic fractions. *Sycp3* (*Synaptonemal complex protein 3*), is strongly expressed in spermatocytes, and is also expressed at low levels in spermatogonia and round spermatids[2]; *Acrv1* (*Acrosomal Vesicle Protein 1*), round spermatid-specific[3]; *Aqp8* (*Aquaporin 8*), condensed spermatid-specific[4]; *β-Act* (*beta actin*), control. (**c**) Western blot analyses of lysates from purified testicular cell fractions confirms that Chd5 is specifically expressed in round spermatids and early elongating spermatids (RS and RES) of $Chd5^{Aam1+/+}$ testes, and is not detected in lysates from other cellular fractions of $Chd5^{Aam1-/-}$ testes. +/+, $Chd5^{Aam1+/+}$; +/-, $Chd5^{Aam1+/-}$; -/-, $Chd5^{Aam1-/-}$.

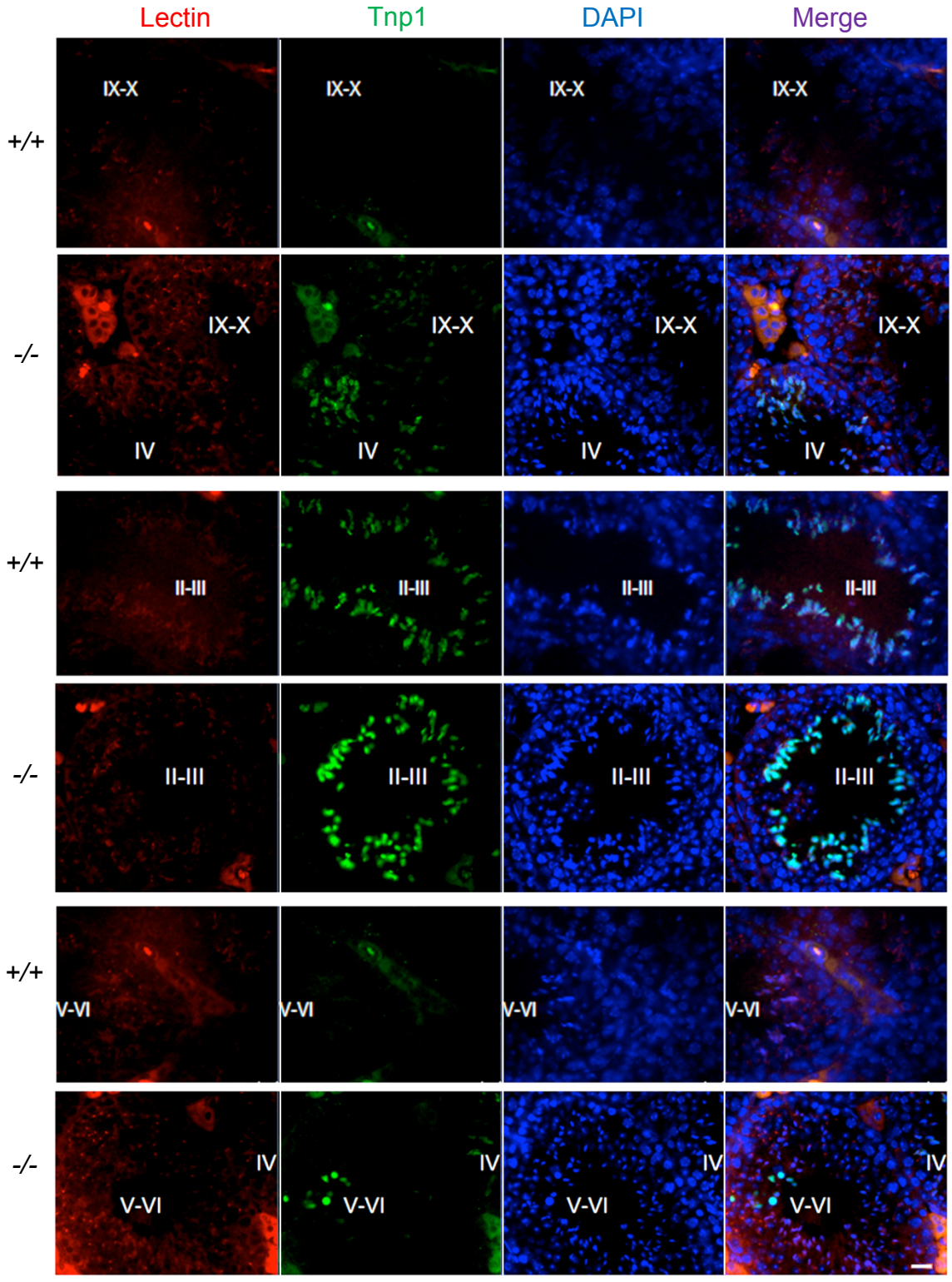
Lectin
Tnp1
DAPI
Merge
+/+
-/-
+/+
-/-
+/+
-/-
IX-X
IV
II-III
V-VI

Supplementary Figure 9. Enhanced and extended Tnp1 expression in Chd5-deficient spermatids

Immunofluorescence for Tnp1 in *Chd5*$^{Aam1+/+}$ (+/+) and *Chd5*$^{Aam1-/-}$(-/-) seminiferous tubules. Roman numerals indicate spermatogenic stages. Red, Lectin (visualizing acrosomes for staging seminiferous tubules); Green, Tnp1; Blue, DAPI. Top panel, Tnp1 is barely detectable in step 9-10 spermatids of stage IX-X tubules of *Chd5*$^{Aam1+/+}$ testes, but is expressed in step 9-10 spermatids in stage IX-X tubules of *Chd5*$^{Aam1-/-}$ testes; middle panel, high Tnp1 expression is detected in step 14 spermatids in stage II-III tubules of both *Chd5*$^{Aam1+/+}$ and *Chd5*$^{Aam1-/-}$ testes, but is expressed more robustly in *Chd5*$^{Aam1-/-}$ tubules; bottom panel, Tnp1 is not detectable in step 15 spermatids of stage V-VI tubules of *Chd5*$^{Aam1+/+}$ testes, but is expressed in step 15 spermatids of stage V-VI tubules of *Chd5*$^{Aam1-/-}$ testes. Scale bar, 20 μm.

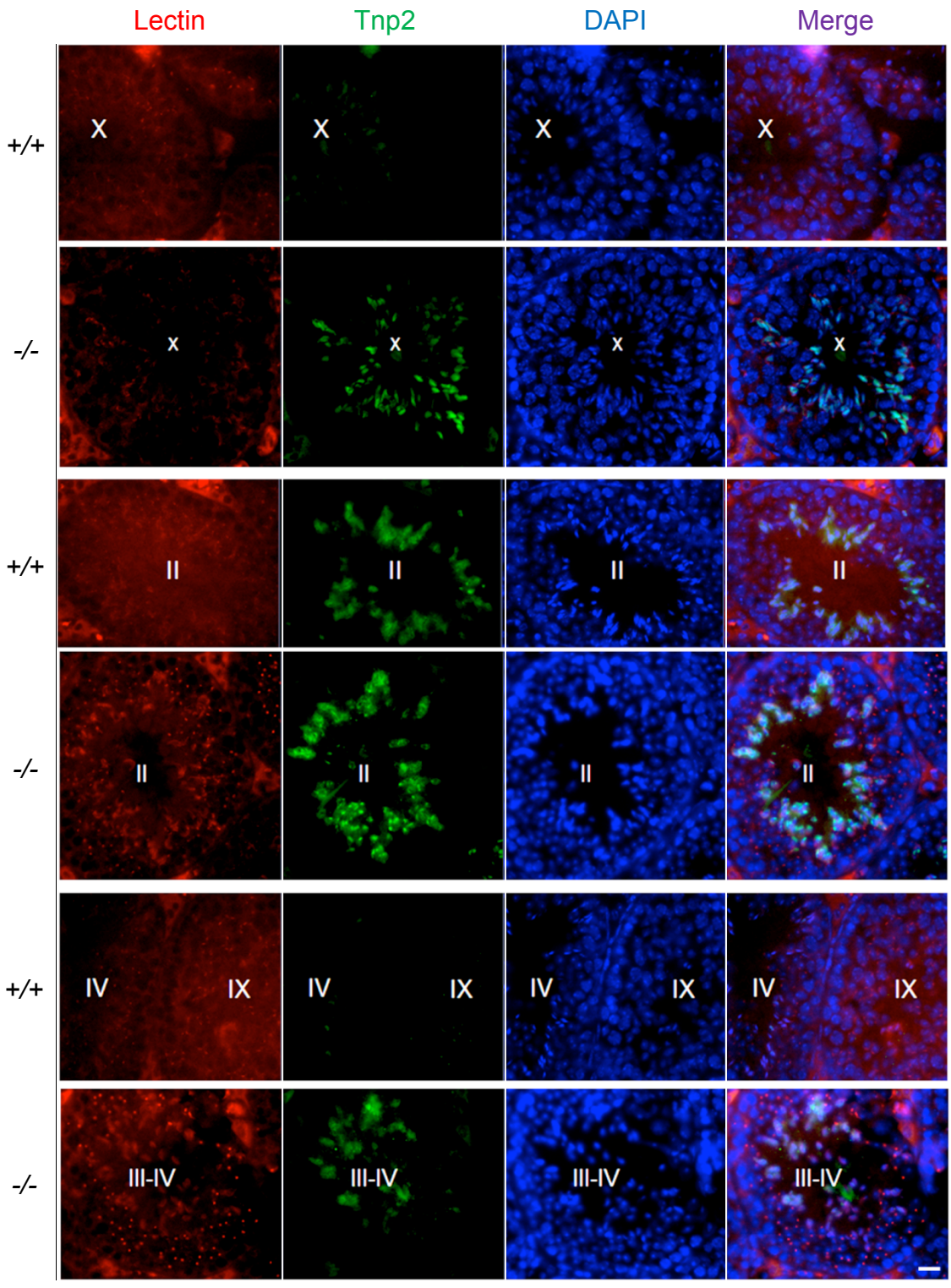
Lectin
Tnp2
DAPI
Merge
+/+
X
X
X
X
-/-
x
x
x
x
+/+
II
II
II
II
-/-
II
II
II
II
+/+
IV
IX
IV
IX
IV
IX
IV
IX
-/-
III-IV
III-IV
III-IV
III-IV

Supplementary Figure 10. Enhanced Tnp2 expression in Chd5-deficient spermatids
Immunofluorescence for Tnp2 in *Chd5*$^{Aam1+/+}$ (+/+) and *Chd5*$^{Aam1-/-}$(-/-) seminiferous tubules. Roman numerals indicate spermatogenic stages. Red, Lectin (visualizing acrosomes for staging seminiferous tubules); Green, Tnp2; Blue, DAPI. Top panel, Tnp2 is first detected in step 10 spermatids of stage X tubules of *Chd5*$^{Aam1+/+}$ testes, but is expressed more intensely in step 10 spermatids of stage X tubules of *Chd5*$^{Aam1-/-}$ tubules; middle panel, high Tnp2 expression is detected in step 14 spermatids of stage II tubules of both *Chd5*$^{Aam1+/+}$ and *Chd5*$^{Aam1-/-}$ testes, but is expressed more intensely in *Chd5*$^{Aam1-/-}$ tubules; bottom panel, Tnp2 becomes weakly detectable in a small portion of step 15 spermatids of stage IV tubules of *Chd5*$^{Aam1+/+}$ testes, but is expressed robustly in step 15 spermatids of stage III-IV tubules of *Chd5*$^{Aam1-/-}$ testes. Scale bar, 20 μm.

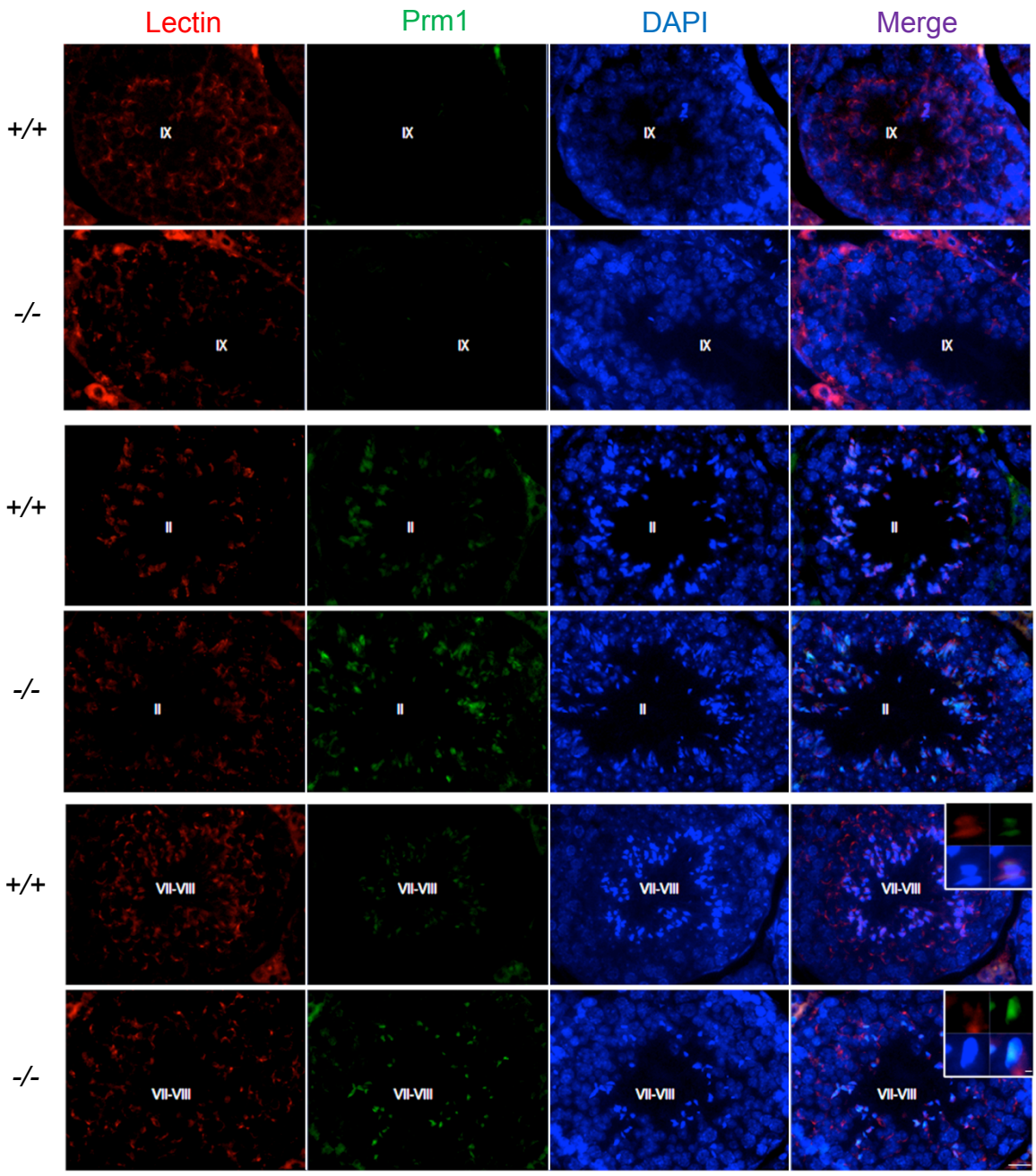
Lectin
Prm1
DAPI
Merge
+/+
-/-
+/+
-/-
+/+
-/-
IX
II
VII-VIII

Supplementary Figure 11. Enhanced Prm1 expression in Chd5-deficient spermatids
Immunofluorescence for Prm1 in *Chd5*$^{Aam1+/+}$ (+/+) and *Chd5*$^{Aam1-/-}$(-/-) seminiferous tubules. Roman numerals indicate spermatogenic stages. Red, Lectin (visualizing acrosomes for staging seminiferous tubules); Green, Prm1; Blue, DAPI. Top panel, Prm1 is not detectable in step 9 spermatids of stage IX tubules of either *Chd5*$^{Aam1+/+}$ or *Chd5*$^{Aam1-/-}$ testes; middle panel, high Prm1 expression is detecatable in step 14 spermatids of stage II tubules in both *Chd5*$^{Aam1+/+}$ and *Chd5*$^{Aam1-/-}$ testes, but is expressed more robustly in *Chd5*$^{Aam1-/-}$ tubules; bottom panel, high Prm1 expression is detectable in step 16 spermatids in stage VII-VIII tubules of both *Chd5*$^{Aam1+/+}$ and *Chd5*$^{Aam1-/-}$ testes, but is expressed more robustly in *Chd5*$^{Aam1-/-}$ tubules. Inserts, high magnification view of representative spermatids of stage VII-VIII tubules. Scale bar, 20 μm and 1 μm for main figure and insert, respectively.

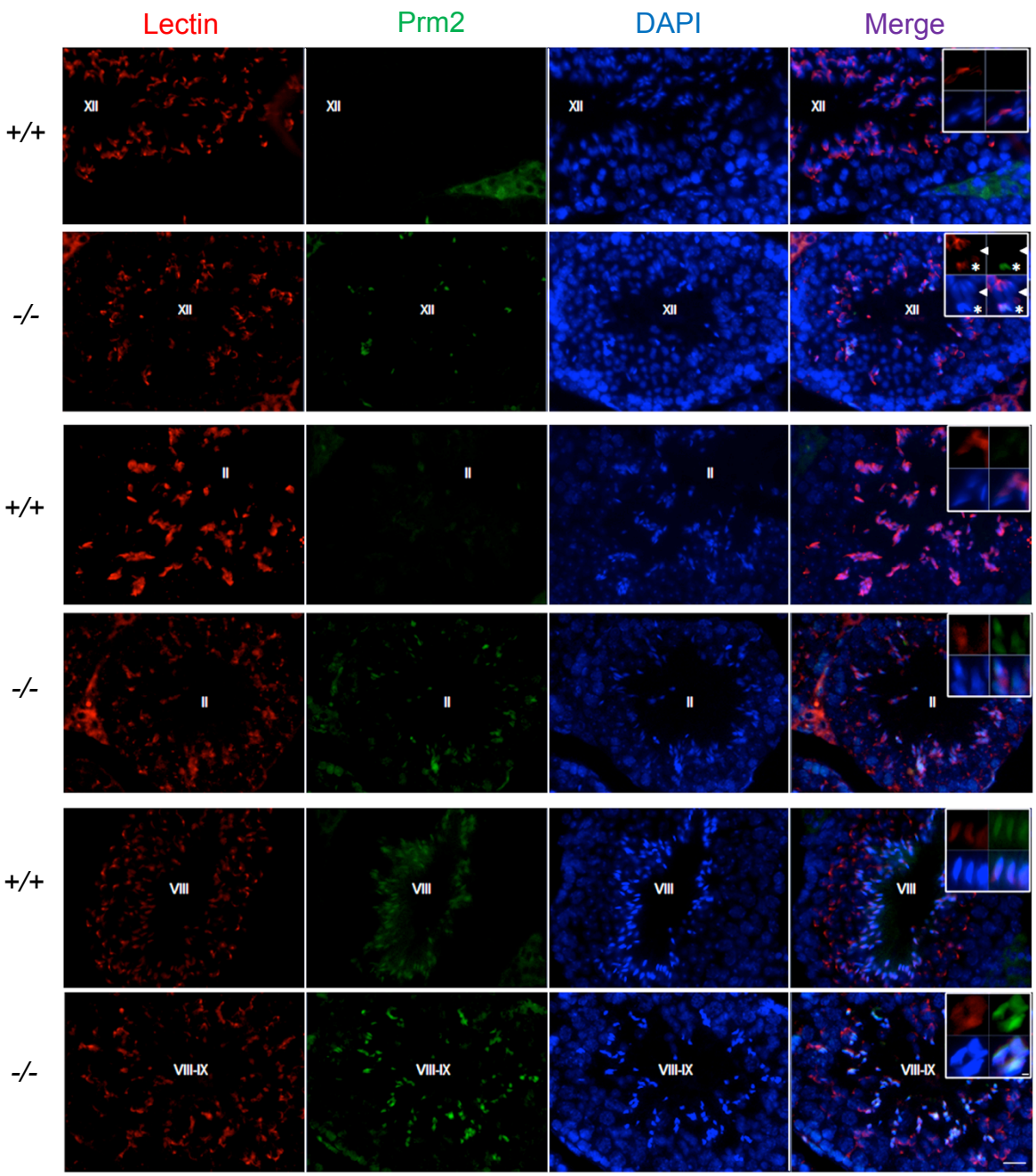
Lectin
Prm2
DAPI
Merge
+/+
-/-
+/+
-/-
+/+
-/-
XII
II
VIII
VIII-IX

Supplementary Figure 12. Enhanced Prm2 expression in Chd5-deficient spermatids
Immunofluorescence for Prm2 in *Chd5*$^{Aam1+/+}$ (+/+) and *Chd5*$^{Aam1-/-}$(-/-) seminiferous tubules. Roman numerals indicate spermatogenic stages. Red, Lectin (visualizing acrosomes for staging seminiferous tubules); Green, Prm2; Blue, DAPI. Top panel, Prm1 is not detected in step 12 spermatids of stage XII tubules of either *Chd5*$^{Aam1+/+}$ or *Chd5*$^{Aam1-/-}$ testes. Inserts, high magnification view of representative spermatids of stage XII tubules. Arrow heads indicate step 12 spermatids which are Prm2-negative. * indicates abnormally retained step16 spermatids which are Prm2-positive. Middle panel, Prm2 is weakly detected in step 14 spermatids of stage II tubules of *Chd5*$^{Aam1+/+}$ testes, but is expressed more intensely in step 14 spermatids of *Chd5*$^{Aam1-/-}$ tubules. Inserts, high magnification views of representative spermatids of stage II tubules. Bottom panel, high Prm2 expression is detected in step 16 spermatids of stage VII-VIII tubules of both *Chd5*$^{Aam1+/+}$ and *Chd5*$^{Aam1-/-}$ testes, but is expressed more robustly in *Chd5*$^{Aam1-/-}$ tubules. Inserts, high magnification view of representative spermatids of stage VII-VIII tubules. Scale bar, 20 μm and 1 μm for main figure and insert, respectively.

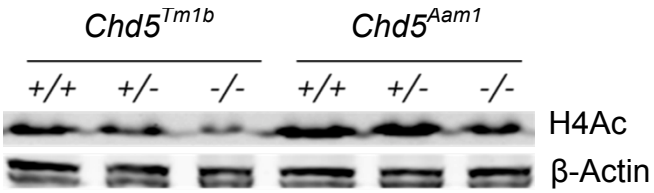

Supplementary Figure 13. Compromised histone H4 acetylation in *Chd5*$^{Tm1b-/-}$ testes
Western blot of total testis lysates indicate a compromise in H4 acetylation (H4Ac) in both *Chd5*$^{Tm1b-/-}$ and *Chd5*$^{Aam1-/-}$ testes relative to wild type, *Chd5*$^{Tm1b+/-}$, and *Chd5*$^{Aam1+/-}$ testes. H4Ac was detected with a rabbit polyclonal antibody against pan-H4 acetylation. β-Actin serves as a loading control.

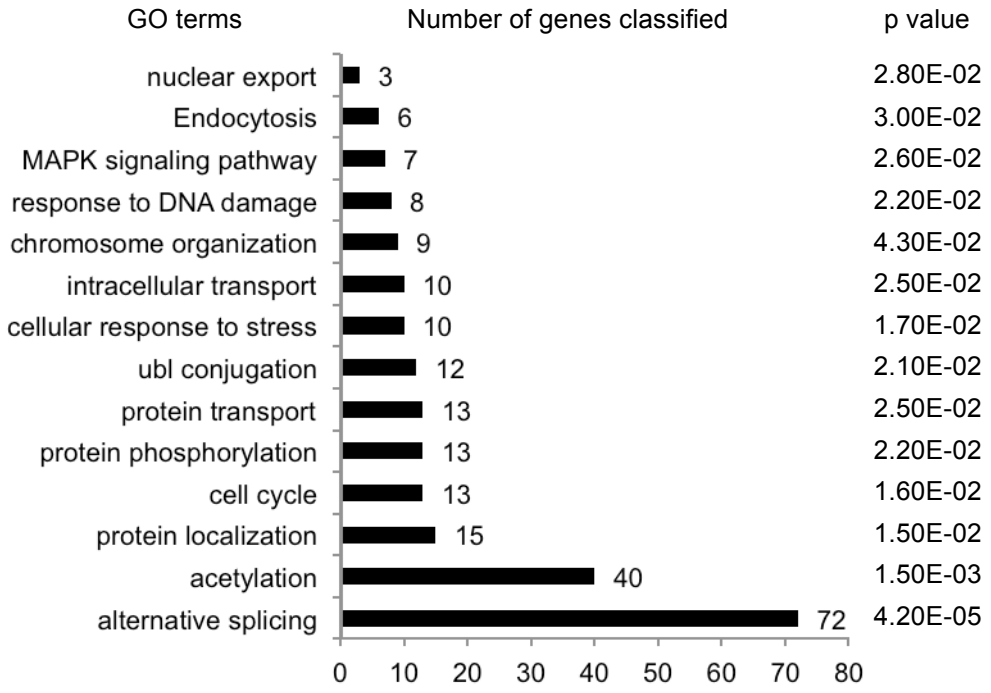

Supplementary Figure 14. Gene ontology analyses of gene expression changes in *Chd5*$^{Aam1-/-}$ round spermatids show enrichment of various GO terms

Gene ontology analyses of the 261 transcripts with a two fold or greater expression change in *Chd5*$^{Aam1-/-}$ round spermatids compared to *Chd5*$^{Aam1+/+}$ counterparts, revealed clustering of a range of GO terms. Numbers next to bars indicate the number of genes classified to the corresponding GO term.

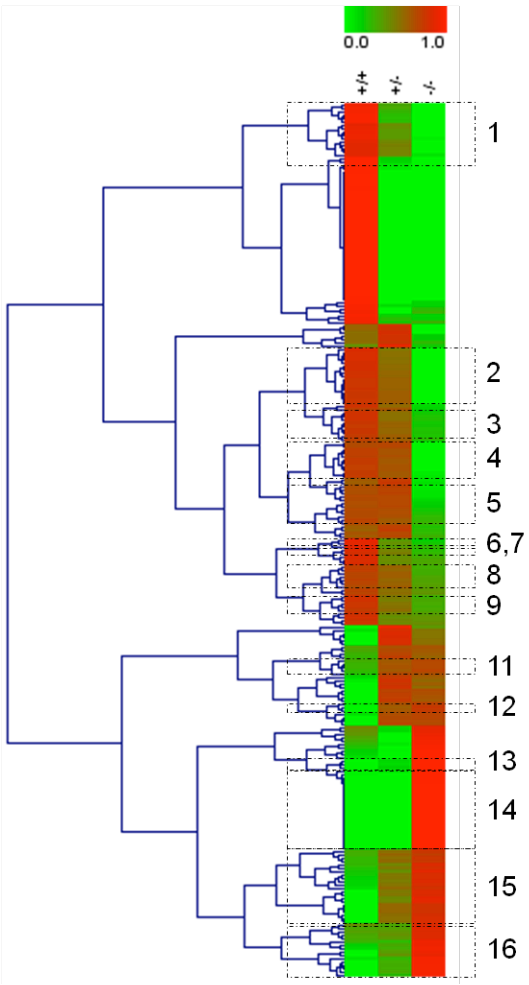

Supplementary Figure 15. Hierarchical clustering and filtration of transcripts showing two fold or more of expression change in *Chd5*$^{Aam1-/-}$ round spermatids
Hierarchical clustering was performed on the 261 transcripts with a two fold or greater expression change in *Chd5*$^{Aam1-/-}$ round spermatids using the clustering tool Genesis (v1.7.6) [5]. Transcripts in cluster 1, 2, 3, 4, 6, 7 and 9 were identified to show gradual expression decrease from *Chd5*$^{Aam1+/+}$ spermatids to *Chd5*$^{Aam1+/-}$ spermatids to *Chd5*$^{Aam1-/-}$ spermatids; transcripts in cluster 11, 12, 13, 15 and 16 were identified to show gradual expression increase from *Chd5*$^{Aam1+/+}$ spermatids to *Chd5*$^{Aam1+/-}$ spermatids to *Chd5*$^{Aam1-/-}$ spermatids; transcripts in clusters 5 and 8 were identified to show an expression decrease in *Chd5*$^{Aam1-/-}$ spermatids but not *Chd5*$^{Aam1+/-}$ spermatids, compared to *Chd5*$^{Aam1+/+}$ spermatids; transcripts in cluster 14 were identified to show expression increase only in *Chd5*$^{Aam1-/-}$ spermatids but not *Chd5*$^{Aam1+/-}$ spermatids compared to *Chd5*$^{Aam1+/+}$ spermatids. Altogether, the 16 clusters identify 155 transcripts that either show gradual expression change in round spermatids across the three genotypes, or that show expression changes specifically in *Chd5*$^{Aam1-/-}$ round spermatids.

a EST profile: Mm.24454 -1700019G17Rik

Tissues	TPM	Gene EST/Total EST
muscle	0	0/27159
nasopharynx	0	0/7955
olfactory mucosa	0	0/3375
ovary	0	0/54858
oviduct	0	0/3825
pancreas	0	0/106229
pineal gland	0	0/3906
pituitary gland	0	0/18069
prostate	0	0/29507
salivary gland	0	0/19385
skin	0	0/118925
spinal cord	0	0/24757
spleen	0	0/92417
stomach	0	0/31760
sympathetic ganglion	0	0/9986
testis	90	11/121820
thymus	0	0/121153
thyroid	0	0/8820
tongue	0	0/11110
turbinate	0	0/1371
uterus	0	0/6855
vagina	0	0/6521
vesicular gland	0	0/2193

b

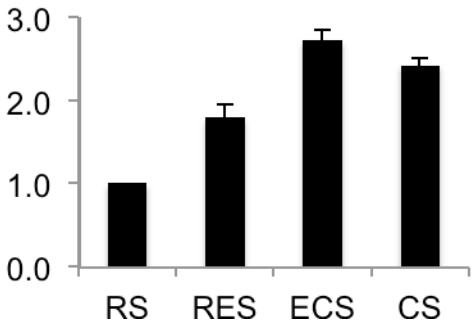

Supplementary Figure 16. Expression profile of *1700019G17Rik*
(**a**) NCBI UniGene EST profile of *1700019G17Rik* (UniGene ID: Mm.24454) shows that *1700019G17Rik* is highly enriched in mouse testis but is absent in many other tissues. TPM, transcripts per million. (**b**) qRT-PCR analyses reveal that *1700019G17Rik* expression increases from round spermatids to elongating spermatids and remains high throughout spermiogenesis in wild type testis. Results are normalized to *Actb* expression. Data are presented as mean ± s.d. from three independent experiments. RS, round spermatids; RES, round and early elongating spermatids; ECS, elongating and condensing spermatids; CS, condensed spermatids.

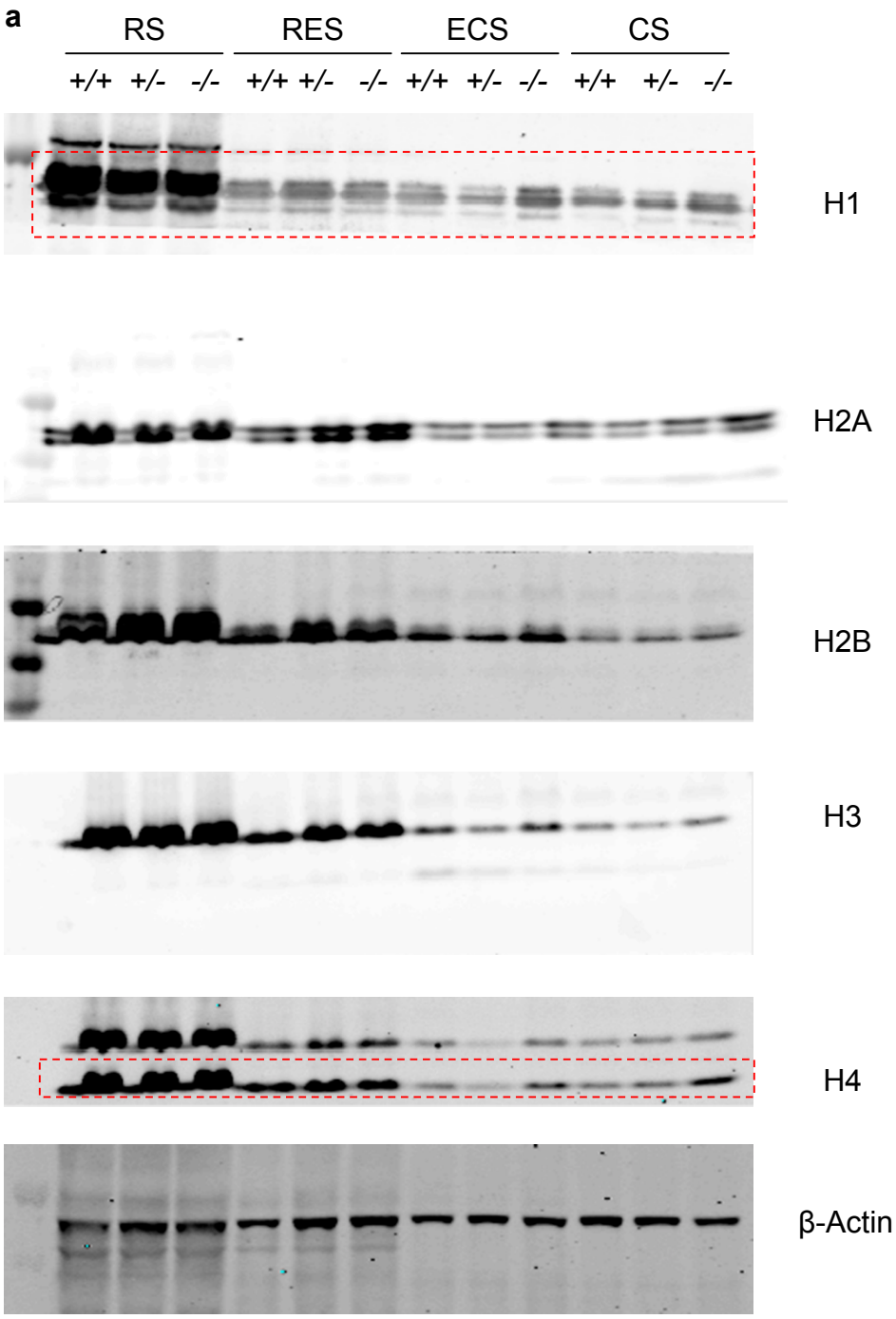
a
RS
RES
ECS
CS
+/+ +/- -/- +/+ +/- -/- +/+ +/- -/- +/+ +/- -/-
H1
H2A
H2B
H3
H4
β-Actin

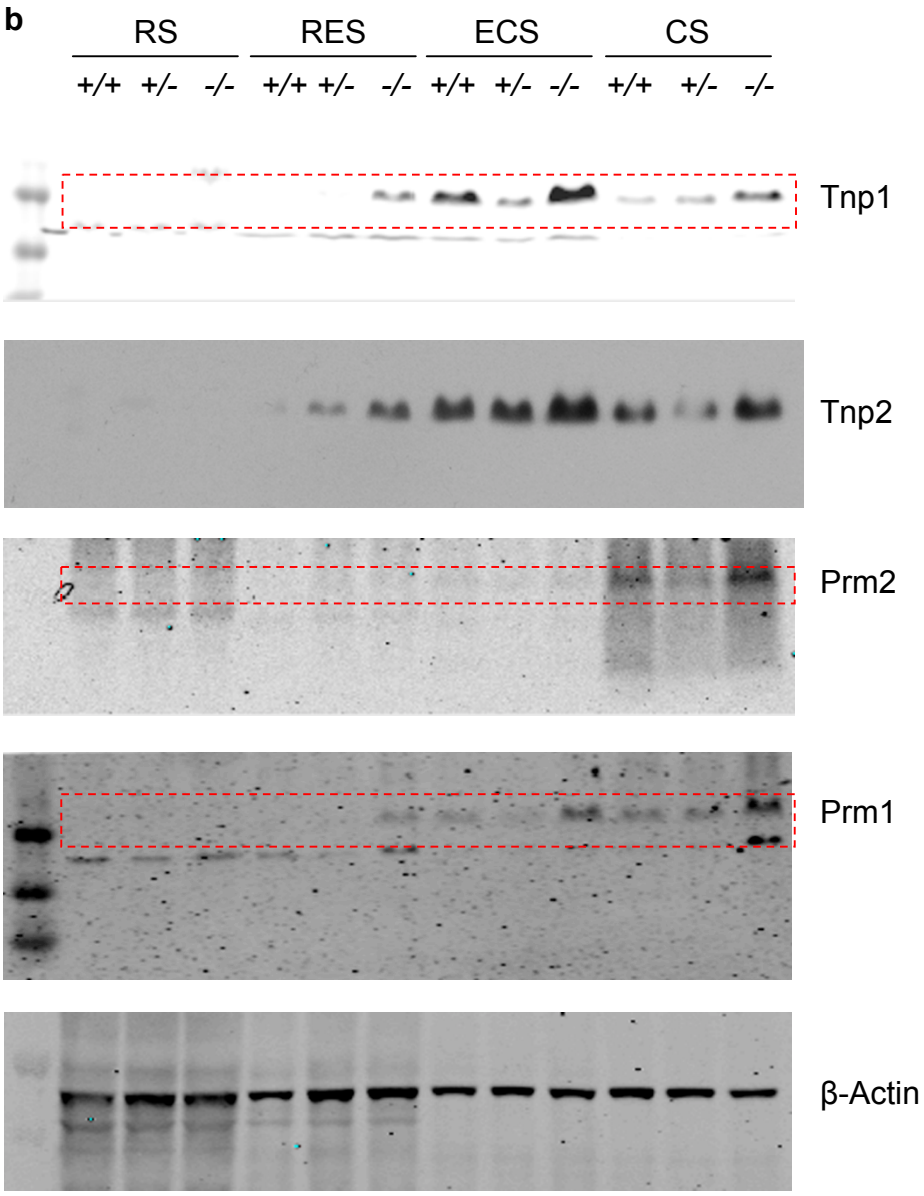
b
RS
RES
ECS
CS
+/+ +/- -/- +/+ +/- -/- +/+ +/- -/- +/+ +/- -/-
Tnp1
Tnp2
Prm2
Prm1
β-Actin
c
+/- +/+ -/-
+/- +/+ -/-
+/- +/+ -/-
+/- +/+ -/-
+/- +/+ -/-
2-Tnp1
2-Tnp2
2-Prm1

Supplementary Figure 17. Western blot scans

(a), (b) Western blot scans of indicated proteins presented in Fig. 3a,b were acquired through ODYSSEY Fluorescent Imaging System (LI-COR) from polyacrylamide gels using fluorescence-conjugated secondary antibodies (LI-COR). **(c)** Scans of indicated gels and Western blots presented in Fig. 3c were acquired through traditional luminescent imaging system from urea-acid gels of basic protein extract. Boxes with red line indicate the target protein bands within the blots. RS, round spermatids; RES, round and early elongating spermatids; ECS, elongating and condensing spermatids; CS, condensed spermatids; +/+, *Chd5*$^{Aam1+/+}$; +/+, *Chd5*$^{Aam1+/+}$; -/-, *Chd5*$^{Aam1-/-}$.

Supplementary Table 1. Mating tests reveal infertility in *Chd5*$^{Aam1-/-}$ male mice

Sex	Genotype	Infertile mice/Total	Fertile mice/Total	Total litter#	Total progeny	Average litter size
Male	*Chd5*$^{Aam1+/+}$	0/8	8/8	24	145	6.0
	Chd5$^{Aam1+/-}$	0/8	8/8	16	104	6.5
	Chd5$^{Aam1-/-}$	4/8	4/8	7	20	2.8
Female	*Chd5*$^{Aam1+/+}$	0/4	4/4	8	52	6.5
	Chd5$^{Aam1-/-}$	0/4	4/4	7	48	6.8

When mated to wild type females for approximately 4 months, 4 out of 8 *Chd5*$^{Aam1-/-}$ male mice tested are infertile. The remaining 4 were sub-fertile, producing only 27.6% (20/72) of the offspring of their *Chd5*$^{Aam1+/+}$ littermates. In contrast, *Chd5*$^{Aam1+/-}$ male mice and *Chd5*$^{Aam1-/-}$ female mice were as fertile as their wild type counterparts.

Supplementary Table 2. Increased abnormal sperm morphology in *Chd5*$^{Aam1-/-}$ mice

Genotype	N	Abnormal sperm morphology	
		Total (%)	Head (%)
Chd5$^{Aam1+/+}$	3	55.7±6.1	32.5±13.6
Chd5$^{Aam1-/-}$	5	85.4±8.6	65.3±7.8
$p_{(+/+ \text{ vs } -/-)}$		0.002*	0.035*

N indicates the number of mice used for the evaluation in each genotype. For each mouse, over 100 sperm were evaluated for morphology. "Total (%)" indicates the percentage of sperm with abnormal morphology in one or more sperm structures, including head, neck, mid-piece and tail. "Head (%)" indicates the percentage of sperm with abnormal head morphology. *p* value is two-tail Student's t-test between the indicated genotypes. +/+, *Chd5*$^{Aam1+/+}$; -/-, *Chd5*$^{Aam1-/-}$; * indicates statistical significance.

Supplementary Table 3. *Chd5*$^{Aam1-/-}$ sperm fail to fertilize wild type oocytes by *in vitro* fertilization

Littermate pairs	Genotype	Sperm used for IVF (million)	Oocytes used for IVF	Oocytes fertilized	Blastocysts developed
1	*Chd5*$^{Aam1+/+}$	0.35	53	23 (43.4%)	17 (32%)
	Chd5$^{Aam1-/-}$	0.35	56	3 (5.4%)	0 (0%)
2	*Chd5*$^{Aam1+/+}$	0.35	114	46 (40.4%)	43 (37.7%)
	Chd5$^{Aam1-/-}$	0.35	108	0 (0%)	0 (0%)
3	*Chd5*$^{Aam1+/+}$	0.35	90	29 (32.2%)	26 (28.9%)
	Chd5$^{Aam1-/-}$	0.35	84	0 (0%)	0 (0%)

An equal number of *Chd5*$^{Aam1+/+}$ and *Chd5*$^{Aam1-/-}$ sperm derived from 3 pairs of littermates were used to fertilize wild type oocytes *in vitro*. The sperm from two *Chd5*$^{Aam1-/-}$ mice failed to fertilize oocytes. Sperm from one *Chd5*$^{Aam1-/-}$ mouse fertilized 5.4% (3/56) of the oocytes, which developed into 2-cell stage but did not develop further. In contrast, sperm from *Chd5*$^{Aam1+/+}$ fertilized 32.2 - 43.4% of the oocytes with 28.9% - 37.7% of the oocytes developing into blastocysts.

Supplementary Table 4. Mating tests revealed infertility in *Chd5*$^{Tm1b-/-}$ male mice

Sex	Genotype	Infertile mice/Total	Fertile mice/Total	Total litter#	Total progeny	Average litter size
Male	*Chd5*$^{Tm1b+/+}$	0/4	4/4	28	220	7.9
	Chd5$^{Tm1b-/-}$	3/5	2/5	5	11	2.2

When mated to wild type females for over 5 months, 3 out of 5 *Chd5*$^{Tm1b-/-}$ male mice tested were infertile. The remaining 2 were subfertile, producing only 5.0% (11/220) of the offspring of their *Chd5*$^{Tm1b+/+}$ littermates. The average of 2.2 progeny per litter produced by subfertile *Chd5*$^{Tm1b-/-}$ male mice is similar to the 2.8 progeny per litter produced by subfertile *Chd5*$^{Aam1-/-}$ male mice (Supplementary Table S1).

Supplementary Table 5. Primer list

Primer	Application	Sequence
Actin-F	qRT-PCR	GATCTGGCACCACACCTTCT
Actin-R	qRT-PCR	GGGGTGTTGAAGGTCTCAAA
Acrv1-F	qRT-PCR	TCAGCAACTTTCAAGCGAGTAT
Acrv1-R	qRT-PCR	CTCCTGAAGAGTGCTCACCTG
Acsl5-F	qRT-PCR	TCCTGACGTTTGGAACGGC
Acsl5-R	qRT-PCR	CTCCCTCAATCCCCACAGAC
Aqp8-F	qRT-PCR	GGATGTCTATCGGTCATTGAG
Aqp8-m	qRT-PCR	GAATTAGCAGCATGGTCTTGA
Car2-F	qRT-PCR	TCCCACCACTGGGGATACAG
Car2-R	qRT-PCR	CTCTTGGACGCAGCTTTATCATA
Cstf2t-F	qRT-PCR	TGGGGAACATTCCGTATGAGG
Cstf2t-R	qRT-PCR	CAGAAGCCATAACCCTTGGG
Gxylt1-F	qRT-PCR	GACGGGCAGGTATGATATGAAAA
Gxylt1-R	qRT-PCR	AAAGCTATCGTGCAGTTGGTC
H1t-F	qRT-PCR	CTGTGGAGGAGAAACCTTCATC
H1t-R	qRT-PCR	GCACCAGGACTCCTTTATTCAC
Hist1h1e-F	qRT-PCR	AGGCAAAGGCAACTAAGGCTA
Hist1h1e-R	qRT-PCR	CTTTAGGCTTTACCGTTTTCGC
Hist1h2bc-F	qRT-PCR	GAGGAGCAGACCTGACATCG
Hist1h2bc-R	qRT-PCR	CACTGTCTTGAGGTTACAGCAT
Hist2h3c1-F	qRT-PCR	AGGACTTCAAGACGGACCTG
Hist2h3c1-R	qRT-PCR	TTTGTGGGGAATGGATGGGA
Klk1b9-F	qRT-PCR	CAACCTATACGAAGAGGAACCCT
Klk1b9-R	qRT-PCR	AGGATGTCGGATGTGGTTTCTA
Pnp2-F	qRT-PCR	CTGCAACACACTGAATATCGACC
Pnp2-R	qRT-PCR	TGGGGAAAGTTGGGTATCTCAT
Prm1-F	qRT-PCR	ACAAAATTCCACCTGCTCACA
Prm1-R	qRT-PCR	GTTTTTCATCGGCGGTGGC
Prm2-F	qRT-PCR	GCTGCTCTCGTAAGAGGCTACA
Prm2-R	qRT-PCR	AGTGATGGTGCCTCCTACATTT
Scara5-F	qRT-PCR	TGGGAAGCTAGGGGCTACG
Scara5-R	qRT-PCR	CGGCAACATTCAGCTCTCTCT
Sik1-F	qRT-PCR	TCATGTCGGAGTTCAGTGCG
Sik1-R	qRT-PCR	ACCTGCGTTTTGGTGACTCG
Sycp3-F	qRT-PCR	AGCCAGTAACCAGAAAATTGAGC
Sycp3-R	qRT-PCR	CCACTGCTGCAACACATTCATA
Syne3-F	qRT-PCR	TGGAGGCAAGGCTTCGAGA

Syne3-R	qRT-PCR	TTCTGGAACCAGCGGTAAAAC
Tnp1-F	qRT-PCR	GAGAGGTGGAAGCAAGAGAAAA
Tnp1-R	qRT-PCR	CCCACTCTGATAGGATCTTTGG
Tnp2-F	qRT-PCR	GAAGGGAAAGTGAGCAAGAGAA
Tnp2-R	qRT-PCR	GCATAGAAATTGCTGCAGTGAC
Trpm8-F	qRT-PCR	ACAGACGTGTCCTACAGTGAC
Trpm8-R	qRT-PCR	GCTCTGGGCATAACCACACTT
Wrnip-F	qRT-PCR	GCAGATCCATCAGCATTAGCA
Wrnip-F	qRT-PCR	GCTCTGGCAAAATAGACCACA
Zfp618-F	qRT-PCR	CCAACCAGTCCCGATCTCC
Zfp618-R	qRT-PCR	GGATTACACTGTTAGGCGTCAAA
1700019G17Rik-F	qRT-PCR	TGCTGACACTACCTCAGACTC
1700019G17Rik-R	qRT-PCR	CAAGAAAGCCAGATAAGGAGCC
28S rRNA-F	qRT-PCR	CCCGACGTACGCAGTTTTAT
28S rRNA-R	qRT-PCR	CCTTTTCTGGGGTCTGATGA
45S rRNA-F	qRT-PCR	ACACGCTGTCCTTTCCCTATTAACACTAAA
45S rRNA-R	qRT-PCR	AGTAAAAAGAATAGGCTGGACAAGCAAAAC
Prm1-5'-F	ChIP-qPCR	CCACAGACGGCACAACT
Prm1-5'-R	ChIP-qPCR	AGTGAGTAGATATGTGCGGATG
Prm1-A-F	ChIP-qPCR	GAATTGGCTGAGGTGGAGTG
Prm1-A-R	ChIP-qPCR	TCACCCTTCTGCCTACCTGT
Prm1-B-F	ChIP-qPCR	GTGCCACACACCTGCTTCTA
Prm1-B-R	ChIP-qPCR	GCAACTCTGAGACCCTCTGG
Prm1-P-F	ChIP-qPCR	TCCTGGTCCTCTTTGACTTCATAAT
Prm1-P-R	ChIP-qPCR	ATCTGCTCCTGCTTTTGCTG
Prm1-C-F	ChIP-qPCR	CTTTTGAAGCCCTTCCCATT
Prm1-C-R	ChIP-qPCR	AGAGCATCTCGCCACATCTT
G-Actin-F	Genotype	GGTCAGAAGGACTCCTATGTGG
G-Actin-R	Genotype	TGTCGTCCCAGTTGGTAACA
Neo-F	Genotype	ATGGGATCGGCCATTGAA
Neo-R	Genotype	GAACTCGTCAAGAAGGCG
Tm1b-F	Genotype	GAGCTAGGCAGGGAAGCAGTGTGG
Tm1b-R	Genotype	CAACGGGTTCTTCTGTTAGTCC
Tm1b-WT-R	Genotype	GGGTGACCTTCAGTTTCTCTGAGC

Supplementary References

1 Namekawa, S. H. *et al.* Postmeiotic sex chromatin in the male germline of mice. *Current biology : CB* **16**, 660-667 (2006).

2 Wang, P. J., Page, D. C. & McCarrey, J. R. Differential expression of sex-linked and autosomal germ-cell-specific genes during spermatogenesis in the mouse. *Human molecular genetics* **14**, 2911-2918 (2005).

3 Reddi, P. P., Flickinger, C. J. & Herr, J. C. Round spermatid-specific transcription of the mouse SP-10 gene is mediated by a 294-base pair proximal promoter. *Biology of reproduction* **61**, 1256-1266 (1999).

4 Yeung, C. H., Callies, C., Rojek, A., Nielsen, S. & Cooper, T. G. Aquaporin isoforms involved in physiological volume regulation of murine spermatozoa. *Biology of reproduction* **80**, 350-357 (2009).

5 Sturn, A., Quackenbush, J. & Trajanoski, Z. Genesis: cluster analysis of microarray data. *Bioinformatics* **18**, 207-208 (2002).